Connecting the Material Parameters of Soft Fibre Reinforced Solids with the Formation of Surface Wrinkles.

A.L. Gower (arturgower@gmail.com)
School of Mathematics, Statistics and Applied Mathematics,
National University of Ireland Galway,
University Road, Galway, Ireland

Abstract.

There is a need for more complete models of fibre reinforced solids that use both anisotropic invariants. However, these models offer major challenges. Two of these challenges are how to combine these anisotropic invariants, and how to reliably determine the models parameters from experiments. We present an intuitive way to account for both anisotropic invariants through a measure of the fibres extension and a measure of the fibres compression. We suggest that a possible remedy to help characterize the material is to use experiments that cause wrinkles to appear on the surface of the material. We call these wrinkles surface-wrinkles.

A soft solid, when compressed, will often develop surface wrinkles within its elastic regime. Much like when we pinch our skin. Here we use the theory of elasticity to effectively model these large deformations and predict the formation of small superimposed wrinkles. Hence we work through the conditions for small surface-wrinkles to appear, and apply these conditions to a simple model that uses both the measures of fibre extension and compression. It turns out that the angle between the fibres and the surface wrinkles orientation can be used to distinguish whether the fibres resist only extension, compression, or a mixture of both.

We also uncover a striking tendency of this angle between the fibres and the wrinkle orientation to alternate between only three or four fixed quanta. This trend increases as the fibres strength is increased.

Keywords: fibre-reinforced, nonlinear elasticity, wrinkles, soft matter.

1. Introduction

Many biological tissues are composed of a soft matrix reinforced by stiffer fibres approximately aligned in one direction at any given point. A most prevalent example is fibres made of collagen embedded in a soft matrix of elastin [1, 2]. If we wish to explore phenomena on a larger scale than the distance between the fibres, then the investigation can be simplified by assuming that the material is homogeneous yet anisotropic with a preferred direction [3].

Much work has been done along this line, with models motivated by specific applications [4], easy to fit to measurements [5], conserving strong-ellipticity [6], and many more. In this work we introduce two anisotropic invariants related to the compression and extension of the fibres, and justify how a simple model based on these invariants addresses a few issues raised in the literature.

The majority of models for the sake of simplicity use only the anisotropic invariant $I_4 = \mathbf{M}^T\mathbf{C}\mathbf{M}$, and leave out the second anisotropic invariant $I_5 = \mathbf{M}^T\mathbf{C}^2\mathbf{M}$, where $\mathbf{C} = \mathbf{F}\mathbf{F}^T$, $\mathbf{F}$ is the deformation gradient and $\mathbf{M}$ is a unit vector aligned with the fibres. It turns out that for these models two of the three shearing modes are identical and infinitesimal shear moduli are all identical, which is not supported by experiments [7]. They are also unlikely to reproduce a certain range of tensile experiments [8], and not allowing an independent contribution from both I_4 and I_5 creates new unrealistic universal relations [9]. We therefore advocate using both anisotropic invariants.

Most models have focused on how the fibres resist extension. However, Ciarletta et al. [6] notes that there is evidence that the presence of fibers alters the mechanical response when under compression, both at the macroscopic [10] and the microscopic levels [11]. To systematically incorporate the fibers' resistance to compression Ciarletta et al. [6] introduced the structural invariant $\mathbf{M}^T(\mathbf{C}+\mathbf{C}^{-1})\mathbf{M}$. However, this structural invariant does not seperate the contributions from both anisotropic invariants. One advantage is that building a strain-energy density from

$\mathbf{M}^T(\mathbf{C}+\mathbf{C}^{-1})\mathbf{M}$ guarantees the condition of *strong-ellipticity* in planar deformations. However, a loss of SE can signal the occurance of several physical phenomenas [12].

To avoid the above limitations, we propose that both anisotropic invariants be included through an invariant that measures the fibres extension $I_4^S = I_4 = \mathbf{M}^T\mathbf{C}\mathbf{M}$ and another that measures the fibres compression $I_4^C = \mathbf{M}^T\mathbf{C}^{-1}\mathbf{M}$. A simple model with these measures has the following anisotropic strain-energy density part

$$W_A = \frac{\mathsf{A}_S}{4}(I_4^S - 1)^2 + \frac{\mathsf{A}_C}{4}(I_4^C - 1)^2, \tag{1}$$

where $\mathsf{A}_S > 0$ and $\mathsf{A}_C > 0$ are constants. This way both invariants I_4 and I_5 are included independently, which is demonstrated in Section 2.1. The larger the value of A_S and A_C, the greater the fibres will resist being stretched and compressed, respectively. This model is a simple prototype, but given the need, more complex models can be developed, such as ones that include the strong stiffening effect observed in collagen [13].

One major challenge for anisotropic models is to be able to reliably determine the models parameters from experiments. Even the protocol for simple tensile testing has not been completely established, as these tests induce shear forces and bending moments [8]. Having both anisotropic invariants further complicates matters, for example it is not possible to fully characterize such a material even with a full range of planar biaxial tests [14].

A possible remedy is to use surface-wrinkling experiments to help characterize the material. We have noticed that varying the fibres resistance to being stretched and compressed creates very distinct wrinkling patterns (Section 3). In essence, wrinkles appear to minimize the strain-energy. When the fibres are stiffer than the surrounding soft matrix, the wrinkles predominantly act to lengthen the fibres, if they resist compression, or shorten the fibres, if they resist extension. This is essentially why varying the contribution from I_4^C and I_4^S to W_A distinctly alters the wrinkling pattern. For a pictorial view of a surface-wrinkle see Figure 2 and [15].

Although the theory behind calculating surface wrinkles is now well established, there is still a scarcity of work investigating this wrinkling of soft anisotropic solids. One notable work [16] investigates the wrinkling of the classic reinforcement model $\mathsf{A}_C = 0$ for simple shear. One major difficulty encountered in that search is how to avoid numerical instabilities. Following along the line of Destrade et al. [16] we use a method based on the surface impedance matrix [17, 18]. In Section 3.2 we present this robust numerical method and demonstrate how it can be reliably used for any choice of anisotropy with one family of fibres. With this method in hand we uncover a striking tendency: the angle between the fibres and the wrinkle orientation alternates between three or four quanta, shown in Figure 6.

Other than determining material parameters, understanding the formation of wrinkling has many technologically applications. For instance, wrinkles are induced to develop functional coatings, such as diffractors or substrates for celular growth [19]. On the other hand, when a material wrinkles it may have reached the limit of its performance [20]. Most applications make use of predictions from linear elasticity, but in the presence of large strain or stress, the nonlinear theory may lead to significantly different outcomes [21]. In this context, the process of wrinkling has contributed to understanding the morphogenesis and the origin of shapes in biological tissues [22, 23].

Wrinkling as a measurement tool has been successfully developed by researchers at the US National Institute of Standards and Technology [24]. This new experimental technique measures the strain needed for thin films to wrinkle, and with this measure determines their elastic modulus. Given the right theoretical and numerical tools, the wrinkling of soft solids can also be used to assist characterize the fibre reinforcement, their orientation and the underlying isotropic matrix. For instance, there is a great interest for such a method to determine the fibres orientation in human skin [25].

The outline is as follows. We explain our choice of fibre reinforcement in Section 2.1, and then develop the relevant incremental equations and the basis for using the Riccati equation

to calculate surface-wrinkles in Section 2.2. To exemplify the numerical method, and as a case study, we present the shear-box deformation in Section 3.1. Using the shear-box as an illustration, the Riccati method for calculating surface-wrinkles is given in Section 3.2. With this method we predict the formation of wrinkles for the shear-box and investigate the results in Section 3.3. Based on the results we suggest asymptotic methods in Section 3.4. We summarize the important features of this paper in Section 4, and give a recap of the phenomena uncovered in the wrinkling pattern, together with directions for possible future work.

2. The Model

2.1. Theoretical Setup

Here we look at the material's response to a large deformation and justify our model of an inclusion of single-family of fibres in a soft matrix. This model is essentially a transverse anisotropic medium. In Section 2.2 we move onto the formation of wrinkles. For more background on the subject of anisotropic nonlinear elasticity see [3].

The behaviour of the material will be determined by our choice of the strain-energy density W. We assume that $W = W_I + W_A$, that is, the sum of an isotropic part and an anisotropic part. For W_I we use a compressible Mooney-Rivlin material,

$$W_I = C_1(I_3^{-1/3}I_1 - 3) + C_2(I_3^{-2/3}I_2 - 3) + \frac{\kappa}{2}(I_3 - 1)^2, \tag{2}$$

where $C_1 > 0$, $C_2 > 0$, $\kappa > 0$ are constants,

$$I_1 = \text{tr } \mathbf{C}, \;\; I_2 = \frac{1}{2}\left[(\text{tr } \mathbf{C})^2 - \text{tr } (\mathbf{C}^2)\right], \;\; I_3 = \det \mathbf{C} = J^2, \tag{3}$$

where $J = \det \mathbf{F}$ and $\mathbf{C} = \mathbf{F}^T\mathbf{F}$ is the right Cauchy-Green strain tensor. For the anisotropic contribution we consider a single family of fibres with their orientation in the reference configuration along the unit vector $\mathbf{M}$, which may vary within the material. We want a simple way to incorporate the fibres resistance to both compression and extension, and we choose,

$$W_A = \frac{\mathsf{A}_S}{4}(I_4^S - 1)^2 + \frac{\mathsf{A}_C}{4}(I_4^C - 1)^2, \tag{4}$$

where

$$I_4^S = \mathbf{M}^T\mathbf{C}\mathbf{M}, \;\; I_4^C = \mathbf{M}^T\mathbf{C}^{-1}\mathbf{M}, \tag{5}$$

and $\mathsf{A}_S > 0$ and $\mathsf{A}_C > 0$ are constants. The square in both the terms of W_A guarantees that W_A is positive, and that the material is stress-free when undeformed, i.e. when $\mathbf{C} = \mathbf{I}$, the Cauchy stress is zero. The invariant I_4^S measures how stretched the fibres are, while I_4^C measures their compression. To justify this statement we decompose $\mathbf{F}$ along the principal directions to obtain

$$\mathbf{F} = \lambda_i \mathbf{v}^i \otimes \mathbf{V}^i, \tag{6}$$

where $\mathbf{v}^i$ and $\mathbf{V}^i$ are unit vectors. When deformed, the fibres orientation and stretch are given by $\mathbf{m}^S = \mathbf{F}\mathbf{M}$ and $\|\mathbf{m}^S\|$ respectively. This can be written as $\mathbf{m}^S = \lambda_i(\mathbf{V}^i \cdot \mathbf{M})\mathbf{v}^i$ and $\|\mathbf{m}^S\|^2 = \lambda_i^2(\mathbf{V}^i \cdot \mathbf{M})^2 = \mathbf{M}^T\mathbf{C}\mathbf{M}$. Here the stretch ratio of the fibre is accounted for by the principal stretches λ_i's. So a term such as $\lambda_i^{-2}(\mathbf{V}^i \cdot \mathbf{M})^2 = \mathbf{M}^T\mathbf{C}^{-1}\mathbf{M}$ would be appropriate to measure the compression ratio of the fibres. This measure is related to the vector $\mathbf{m}^C = \mathbf{F}^{-T}\mathbf{M} = \lambda_i^{-1}(\mathbf{V}^i \cdot \mathbf{M})\mathbf{v}_i$ because $\|\mathbf{m}^C\|^2 = \mathbf{M}^T\mathbf{C}^{-1}\mathbf{M}$. Note that using $\mathbf{M}^T\mathbf{C}^{-1}\mathbf{M}$ rather than $1/(\mathbf{M}^T\mathbf{C}\mathbf{M})$ leads to simpler algebraic expressions.

For any model of anisotropy to reproduce a range of experiments, both the classical invariants, commonly name $I_4 = I_4^S$ and $I_5 = \mathbf{M}^T\mathbf{C}^2\mathbf{M}$, must have an independent contribution to the strain-energy density W. This condition is respected for any strain energy that has an independent contribution from I_4^S and I_5^S, such as W_A. We show this statement by applying the CayleyHamilton theorem to $\mathbf{C}$ to get

$$\mathbf{C}^3 - \mathbf{C}^2 I_1 + \mathbf{C} I_2 - I_3 = 0 \implies \mathbf{C}^2 - \mathbf{C} I_1 + I_2 - \mathbf{C}^{-1} I_3 = 0, \tag{7}$$

multiplying by $\mathbf{M}^T$ on the left side and $\mathbf{M}$ on the right side, and then rearranging, we reach

$$I_5 = I_5^S I_3 + I_4^S I_1 - I_2. \tag{8}$$

As $I_3 \neq 0$, both I_5 and I_4 are independently accounted for in W_A. The papers [6, 25] use the structural invariant $I_\alpha = I_4^S + I_4^C - I$, and fixing $\mathsf{A}_C = 0$ is known as the standard fibre reinforcement model [8].

Now consider that the material is deformed by taking a material point initially at $\boldsymbol{X}$ in the reference configuration to position $\boldsymbol{x} = \boldsymbol{x}(\boldsymbol{X})$ in the current configuration. Let (X_1, X_2, X_3) and (x_1, x_2, x_3) be fixed rectangular Cartesian coordinates of $\boldsymbol{X}$ and $\boldsymbol{x}$, respectively. The Cauchy stress tensor $\boldsymbol{\sigma}$ is then given by the connection [26, 27]

$$\sigma_{ij} = J^{-1} \frac{\partial W}{\partial F_{ia}} F_{ja}, \tag{9}$$

where $F_{ij} = \partial x_i / \partial X_j$. Through our choice $W = W_I + W_A$ we can separate the stress into

$$\sigma_{ij} = \sigma_{ij}^I + \sigma_{ij}^A, \tag{10}$$

where

$$\sigma_{ij}^I = J^{-1} \frac{\partial W_I}{\partial F_{ia}} F_{ja} \quad \text{and} \quad \sigma_{ij}^A = J^{-1} \frac{\partial W_A}{\partial F_{ia}} F_{ja}. \tag{11}$$

Introducing $\mathbf{m}^C = \mathbf{F}\mathbf{M}$ and $\mathbf{m}^S = \mathbf{F}^{-1}\mathbf{M}$ we find that

$$\sigma_{ij}^A = J^{-1} \left(\mathsf{A}_S (I_4^S - 1) m_i^S m_j^S - \mathsf{A}_C (I_4^C - 1) m_i^C m_j^C \right), \tag{12}$$

and

$$\sigma_{ij}^I = -p\delta_{ij} + 2\left(C_2 I_1 + C_1\right) B_{ij} - 2C_2 B_{i\beta_1} B_{j\beta_1}, \tag{13}$$

for an incompressible solid, where p is a Lagrange multiplier due to the constraint $\det F = 1$ at all times. For a compressible solid we find

$$\sigma_{ij}^I = -\left(\frac{2}{3} C_1 I_1 I_3^{-1/3} + \frac{4}{3} C_2 I_2 I_3^{-2/3} - 2\kappa (I_3 - 1) I_3 \right) \delta_{ij} + 2\left(C_2 I_1 I_3^{-2/3} + C_1 I_3^{-1/3} \right) B_{ij} - 2C_2 I_3^{-2/3} B_{i\beta_1} B_{j\beta_1}.$$

The compressible version of $\boldsymbol{\sigma}^I$ is more involved but also more general. The method we present in Section 2.2 is for compressible solids, though because we focus on almost incompressible solids, the simpler incompressible equations can be useful.

To see how this model of anisotropy influences the stress response, we take a uniaxial isochoric deformation parallel to the fibers $F_{ij} = \lambda M_i M_j + \lambda^{-1} M_i^\perp M_j^\perp$, with the unit vector $\mathbf{M}^\perp$ perpendicular to $\mathbf{M}$, leading to

$$\sigma_{ij}^A = \left[\lambda^2 \mathsf{A}_S (\lambda^2 - 1) - \lambda^{-2} \mathsf{A}_C (\lambda^{-2} - 1) \right] M_i M_j.$$

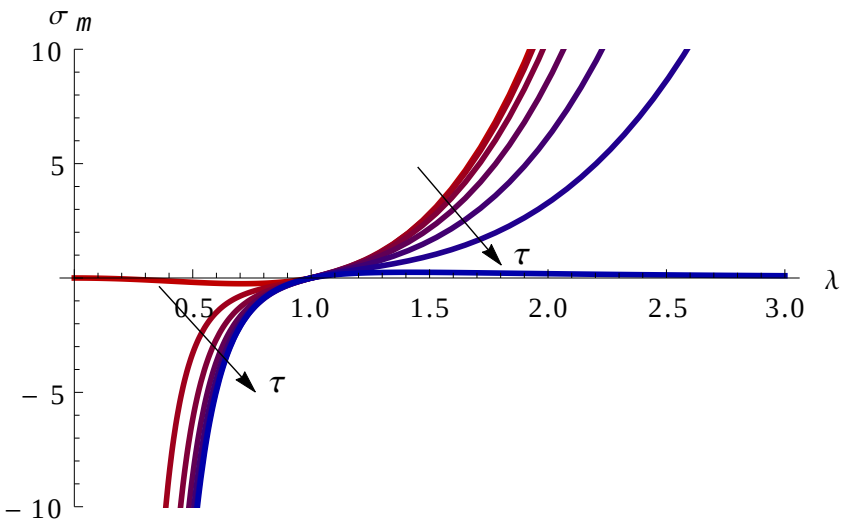

Figure 1. The ratio of uniaxial deformation λ against the stress σ_m, both taken along the fibre orientation $\mathbf{M}$. Each curve corresponds to a different value for τ where $\mathsf{A}_S = \cos\tau$ and $\mathsf{A}_C = \sin\tau$. As the curves shade from red to blue (indicated by the arrows), τ increase from 0 to $\pi/2$ by increments of $\pi/12$, and the material offers less resistence to extension and more resistence to compression.

To illustrate we plot several curves of $\sigma_m = \sigma^A_{ij} M_j M_i$ against λ, see Figure 1.

2.2. Incremental Equations

To reach the conditions for small amplitude surface-wrinkles to appear on top of a large elastic deformation, we need to first work through the incremental equations of stress and equilibrium. Then we must apply these equations to a surface-wrinkle. We do this in a simple setting where the material occupies the half-space $x_2 \geq 0$, and we take the boundary $x_2 = 0$ to be free of traction. A small-amplitude wrinkle in this material is described by the displacement field $\mathbf{u} = \mathbf{u}(\boldsymbol{x})$, satisfying in the cartesian coordinate system (x_1, x_2, x_3) the incremental equations of equilibrium [26],

$$s_{pj,p} = \mathcal{A}_{pjq\ell} u_{\ell,pq} = 0 \quad \text{with} \quad \mathcal{A}_{pjq\ell} = \frac{1}{J} F_{pa} F_{qb} \frac{\partial^2 W}{\partial F_{ja} \partial F_{\ell b}} = \mathcal{A}^I_{pjq\ell} + \mathcal{A}^A_{pjq\ell}, \tag{14}$$

where $s_{pi} = \mathcal{A}_{piqj} u_{j,q}$ are the components of the incremental nominal stress tensor, $\mathcal{A}^I_{pjq\ell}$ and $\mathcal{A}^A_{pjq\ell}$ are respectively the contribution to $\mathcal{A}_{pjq\ell}$ from W_A and W_I. We assume that in the region of dead-load stability, see [26], $\boldsymbol{\mathcal{A}}$ satisfies the *strong-convexity* condition (S-C)

$$\mathcal{A}_{ijk\ell} \xi_{ij} \xi_{k\ell} > 0 \quad \text{for all non-zero matrices } \boldsymbol{\xi}. \tag{15}$$

The *strong-ellipticity* condition reads

$$\mathcal{A}_{paqb} v_p v_q w_a w_b > 0 \quad \text{for all non-zero vectors } \mathbf{v} \text{ and } \mathbf{w}, \tag{16}$$

and is implied by strong-convexity. For an interpretation of strong-ellipticity see [28, 12]. Using W_A from equation (4) and $(14)_2$ we find that

$$\begin{aligned} \mathcal{A}^A_{ijk\ell} = \mathsf{A}_C \left[(I^C_4 - 1) \left(\delta_{jk} m^C_i m^C_\ell + \delta_{ik} m^C_j m^C_\ell + \delta_{i\ell} m^C_j m^C_k \right) + 2 m^C_i m^C_j m^C_k m^C_\ell \right] \\ + \mathsf{A}_S \left[(I^S_4 - 1) \delta_{j\ell} m^S_i m^S_k + 2 m^S_i m^S_j m^S_k m^S_\ell \right]. \end{aligned} \tag{17}$$

A wrinkle along the surface $x_2 = 0$ with wrinkle-front normal to $\mathbf{n}$ direction is of the form

$$\mathbf{u}(x_1, x_2, x_3) = \mathbf{U}(x_2)\mathrm{e}^{\mathrm{i}k\boldsymbol{x}\cdot\boldsymbol{n}}, \tag{18}$$

where the amplitude $\mathbf{U}$ is a vector function of x_2 alone, k is the wavenumber and $\boldsymbol{n} = (\cos\theta, 0, \sin\theta)$. We can think of $\mathbf{U}$ as the result of a Fourier transform in x_1 and x_3, implying that solving $\mathbf{U}$ for every θ will form a complete basis for first-order bifurcation. For $\mathbf{u}$ to satisfy the equations of motion $(14)_1$ for every x_1 and x_3 we must have

$$\mathsf{T}\mathbf{U}''(x_2) + \mathrm{i}k(\mathsf{R} + \mathsf{R}^{\mathrm{T}})\mathbf{U}'(x_2) - k^2\mathsf{Q}\mathbf{U}(x_2) = \mathbf{0}, \tag{19}$$

where the matrices R, Q,T are given by

$$\mathsf{T} = \mathsf{Q}^{\{2\}}, \quad \mathsf{R} = \mathsf{R}^{\{3\}}\cos\theta + \mathsf{R}^{\{1\}}\sin\theta, \tag{20}$$

$$\mathsf{Q} = \mathsf{Q}^{\{1\}}\cos^2\theta + \mathsf{Q}^{\{3\}}\sin^2\theta + (\mathsf{R}^{\{2\}} + \mathsf{R}^{\{2\}\mathrm{T}})\cos\theta\sin\theta, \tag{21}$$

which in turn are defined in terms of their components by

$$\begin{aligned} &Q^{\{1\}}_{j\ell} = \mathcal{A}_{1j1\ell}, \quad Q^{\{2\}}_{j\ell} = \mathcal{A}_{2j2\ell}, \quad Q^{\{3\}}_{j\ell} = \mathcal{A}_{3j3\ell}, \\ &R^{\{1\}}_{j\ell} = \mathcal{A}_{2j3\ell}, \quad R^{\{2\}}_{j\ell} = \mathcal{A}_{3j1\ell}, \quad R^{\{3\}}_{j\ell} = \mathcal{A}_{2j1\ell}, \\ &Q_{j\ell} = \mathcal{A}_{pjq\ell}n_p n_q, \quad R_{j\ell} = \mathcal{A}_{2jq\ell}n_q, \end{aligned} \tag{22}$$

where $Q^{\{n\}}_{ij} = Q^{\{n\}}_{ji}$ for $n = 1, 2$ and 3. The matrices $\mathsf{Q}^{\{1\}}$, $\mathsf{Q}^{\{2\}}$, $\mathsf{Q}^{\{3\}}$ and Q are positive definite due to strong-ellipticity (16).

A surface-wrinkle is simply a wrinkle that decays as x_2 increases, that is

$$\lim_{x_2\to\infty} \mathbf{U}(x_2) = 0. \tag{23}$$

To satisfy this condition it is well established, see [29], that the general solution to the ODE (19) is of the form

$$\mathbf{U}(x_2) = \mathrm{e}^{\mathrm{i}k\mathsf{E}x_2}\mathbf{U}_0 \tag{24}$$

where $\mathbf{U}_0$ is a constant vector and E is a constant 3 x 3 matrix (not to be confused with the Green strain) whose eigenvalues have a positive imaginary part, i.e. Im Spec $\mathsf{E} > 0$. Such an E always exists if strong-ellipticity holds.

Figure 2 illustrates a surface wrinkle and how its amplitude decays when moving away from the surface (as x_2 increases).

The resulting incremental traction $s_{pi} = \mathcal{A}_{piqj}u_{j,q}$ due to the wrinkle $\mathbf{u}$ is

$$s_{2i} = \mathrm{i}k(\mathsf{R}_{ij} + \mathsf{T}_{ia}\mathsf{E}_{aj})u_j. \tag{25}$$

For the surface $x_2 = 0$ to have zero traction, then $s_{2i} = 0$ for $i = 1$, 2 and 3, which in turn implies that $\det(\mathsf{R} + \mathsf{TE}) = 0$. Now rather than solving for E with Im Spec $\mathsf{E} > 0$, and that satisfies the above condition, a successful method is to solve directly for the *impedance matrix*

$$\mathsf{Z} = -\mathrm{i}(\mathsf{R} + \mathsf{TE}), \quad \text{where} \quad s_{2i} = -k\mathsf{Z}_{ij}u_j. \tag{26}$$

The impedance matrix relates the incremental displacement to the incremental normal traction, as shown above, which leads to many useful properties [17, 21, 30]. The decay condition Im Spec $\mathsf{E} > 0$ is equivalent to $\mathsf{Z} = \mathsf{Z}^{\dagger}$ together with $\mathsf{Z} > 0$, where the superscript † denotes the Hermitian, both these properties can be shown through balance of virtual momentum [21]. A traction free surface is guaranteed if $\det\mathsf{Z} = 0$. To solve for Z we substitute $\mathsf{E} = \mathrm{i}\mathsf{T}^{-1}(\mathsf{Z} + \mathrm{i}\mathsf{R})$ and the form (24) into the ODE (19), to reach the algebraic Riccati equation

$$(\mathsf{R}^{\mathrm{T}} + \mathrm{i}\mathsf{Z})\mathsf{T}^{-1}(\mathsf{R} - \mathrm{i}\mathsf{Z}) - \mathsf{Q} = 0, \tag{27}$$

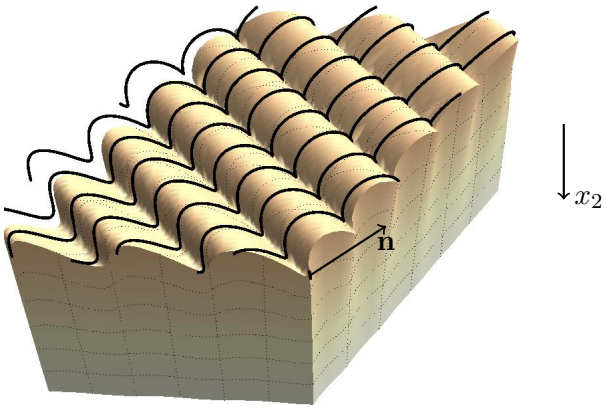

Figure 2. An illustration of a surface-wrinkle on a fibre reinforced material, with $\mathbf{n}$ being normal to the wrinkle-front. The curvy black lines indicate the fibre angle. Note that the surface-wrinkle's amplitude decays as x_2 increases.

which has a unique solution for a positive definite Z (i.e. $\mathsf{Z} > 0$). Because Z is hermitian we can rewrite the Riccati equation (27) as

$$(\mathsf{R}^{\mathrm{T}} + \mathrm{i}\mathsf{Z})\mathsf{T}^{-1/2}\left[(\mathsf{R}^{\mathrm{T}} + \mathrm{i}\mathsf{Z})\mathsf{T}^{-1/2}\right]^{\dagger} = \mathsf{Q}, \tag{28}$$

There are efficient numerical methods to solve the Riccati equation based on Schur decomposition [31], Newton method [32] and more recently the matrix sign function [33].

In conclusion, a surface-wrinkle with zero surface traction corresponds to

$$\mathsf{Z} \geq 0\,(\text{positive semi-definite}), \quad \mathsf{Z} = \mathsf{Z}^{\dagger} \quad \text{and} \quad \det \mathsf{Z} = 0. \tag{29}$$

A similar use of the Riccati equation to find a zero-traction solution was originally developed for surface-waves [34]. In Section 3.2 we describe how best to use the Riccati equation to locate a traction free surface-wrinkle.

3. Shear-Box Wrinkling

3.1. The Shear-box

To obtain a large homogeneous static deformation, we use the *shear-box deformation* [35], see Figure 3. Other experimental tests such as the finite bending test [36] and simple tension experiments [8] can become more involved when the experimental setup does not reflect the symmetries of the material. The shear-box deformation brings a point with material coordinates (X_1, X_2, X_3) to the spatial position with coordinates (x_1, x_2, x_3) given by

$$x_1 = X_1 + X_3 \sin\varphi, \qquad x_2 = \lambda_2 X_2, \qquad x_3 = X_3 \cos\varphi, \tag{30}$$

where φ is the *tilting angle*: at $\varphi = 0$, the box is rectangular; at $\varphi = 90°$, it is flattened. To achieve this deformation we imagine that the inner walls of the shear-box are lubricated so that the soft material placed within may slide. This way, when the box is tilted, the material can expand its height in the x_2 coordinate uniformly. To achieve a homogeneous deformation we also assume that the fibres are parallel to the free-surface $x_2 = 0$, a common occurance in biological tissues. So we may write $\mathbf{M} = (\cos A, 0, \sin A)$, this in turn leads to the stress on the surface

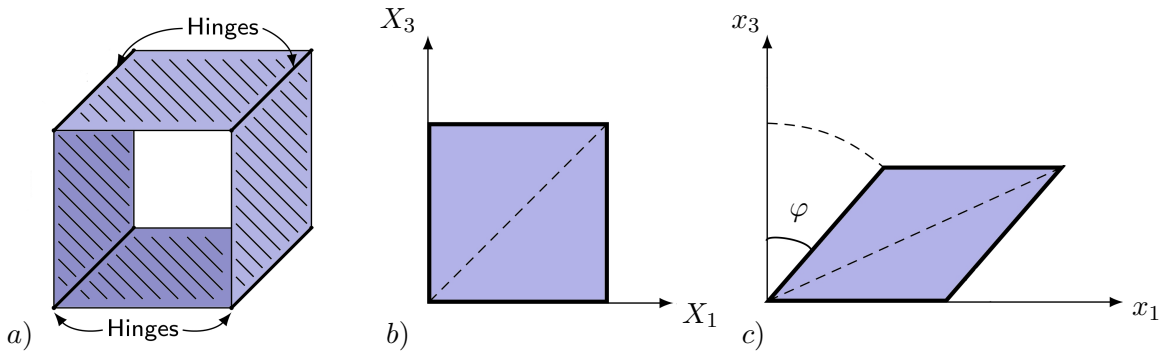

Figure 3. A schematic of the shear-box deformation.

$x_2 = 0$, σ_{i2}, being zero all except the normal component σ_{22}. So we determine the principal stretch λ_2 by solving $\sigma_{22} = 0$ in terms of φ, which leads to

$$C_1\left(1-\lambda_2^2\right) + C_2\left(\lambda_2\cos\varphi\right)^{-2/3}\left(\cos^2\varphi - \lambda_2^2\right) + \frac{3}{2}\kappa(\lambda_2\cos\varphi)^{8/3}\left(1-\lambda_2^2\cos^2\varphi\right) = 0, \qquad (31)$$

which must be solved numerically. For an incompressible material $\lambda_2 = (\cos\varphi)^{-1}$, and for κ a hundred times larger than $C_1 + C_2$ for a compressible material, we find that $\lambda_2 \approx (\cos\varphi)^{-1}$ with a maximum error of 1% for $\phi < 60°$, which is within the range of our numerical experiments.

The shear-box is a simple example for it needs only the tilting angle φ to control the deformation, and it is viable to execute experimentally. In contrast, a biaxial test has many parameters and can be difficult to achieve in-plane for fibre reinforced solids [14]. With the shear-box deformation we will illustrate our method for calculating surface wrinkles and our asymptotic results.

3.2. The Riccati Method

The essence of the method is to deform the material step-by-step and check, at each step, whether the material can now sustain a surface-wrinkle. To describe surface wrinkles we use the incremental framework developed in Section 2.2, and let the magnitude of the finite deformation be parametrized by φ, with $\varphi = 0$ corresponding to no deformation (such as the tilt angle φ for the shear-box deformation).

To run the numerical method, the material constants C_1, C_2, κ, A_S and A_C in equations (2) and (4) must first be fixed. At this point the incremental moduli $\mathcal{A}_{ijkl}$, given in equations $(14)_2$, are a function of the magnitude of the deformation φ, the angle of the wrinkle-front θ, used in equation (18), and the angle of the fibres A. Note that $\mathbf{M} = (\cos A, 0, \sin A)$. So the matrices $\mathbf{T} = \mathbf{T}(\varphi,\theta,A)$, $\mathbf{R} = \mathbf{R}(\varphi,\theta,A)$ and $\mathbf{Q} = \mathbf{Q}(\varphi,\theta,A)$ made up from the components of $\mathcal{A}_{ijkl}$ are also functions of φ, θ and A. These matrices determine a unique positive definite $\mathbf{Z}$ through the Riccati equation (27), so that $\mathbf{Z}$ is also a function of φ, θ, and A. For there to exist an initial positive definite $\mathbf{Z}$ for $\varphi = 0$, the strong-convexity condition (15) must hold.

Below we calculate the first surface-wrinkle to appear. To do so, for each fibre angle A, we increase the deformation until we reach a critical amount $\varphi = \varphi^*(A)$, at which point $\det\mathbf{Z} = 0$, meaning that there exists a zero traction surface-wrinkle with $\theta = \theta^*(A)$. The method is detailed below.

The Riccati method

For each fibre orientation $A \in [0, \pi]$, set $\varphi = 0$ then

1. Calculate for every $\theta \in [0, \pi]$ the positive semi-definite Hermitian $\mathbf{Z}$.

2. If $\det \mathbf{Z} > tol$ for every $\theta \in [0, \pi]$, then increment φ and go back to **1.**

3. Find θ such that $\det \mathbf{Z}$ is a minimum, and set $\theta^*(A) = \theta$ and $\varphi^*(A) = \varphi$.

At the end of the process we have a curve $(\varphi^*(A), \theta^*(A))$ giving the deformation magnitude and angle of the wrinkle-front as a function of the fibre angle A.

Methods based on looking for positive semi-definite solutions for $\mathbf{Z}$ can be difficult to use. This is mainly due to the $\det \mathbf{Z}$ being very sensitive to small variations in φ, θ and A. So, at Step **2.** the error tolerance *tol* would have to be much larger than the mesh size of φ and θ. Otherwise, at Step **1.**, after an increment in φ, we may step past the zero-traction solution and simply find no positive semi-definite solution for some θ. It is also possible not to find a positive semi-definite $\mathbf{Z}$ because there is no surface-wrinkle for A. To distinguish between the two cases, it would be necessary to decrease φ very thinly to investigate which situation occured.

This problem can be circumvented by using a method based on implicitly solving for $\mathbf{Z}$, without taking into consideration $\mathbf{Z}$ being positive semi-definite. These implicit solutions should begin at the positive definite $\mathbf{Z}$ for $\varphi = 0$, but then as φ is increased one should seek solutions to $\mathbf{Z}$ implicitly by using the Riccati equation (27), without explicitly looking for positive definiteness. The uniqueness of a positive semi-definite $\mathbf{Z}$ means that the implicit solutions will be well defined, and that when $\det \mathbf{Z} < 0$, with Hermitian $\mathbf{Z}$, we are sure that a zero-traction surface-wrinkle exists, and is close by.

We note, however, that numerically for the model in question, a surface-wrinkle exists for every fiber orientation, within the parameters we explored. To verify the correctness of the algorithm, we also reproduced the results found in [25, 16].

3.3. Predictions

For our simulations, we will set the material parameters in (2) to be $C_1 = 1$, $\kappa = 200$ (to make the material virtually incompressible), and will study the effect of varying C_2 and varying the fibres resistance to stretch A_S and to compression A_C in (4). To control the fibre strength and resistance to stretch/compression separately we set $(\mathsf{A}_S, \mathsf{A}_C) = (\mathsf{S}\cos\tau, \mathsf{S}\sin\tau)$, where S is a constant.

For the standard fibre reinforcement model, $\mathsf{A}_C = 0$ and $C_2 = 0$, the ratio of the fibre strength has been estimated to be $\mathsf{S}/C_1 = 20, 40, 80$ for several biological tissues [16]. So we will investigate the stability of fibre strength around the same order and take the values $\mathsf{S} = 16$, 32, and 64. For simplicity we begin by setting $C_2 = 0$, $C_1 = 1$. The wrinkling patterns for $\mathsf{S} = 16$ are shown in Figure 4, with $\tau = 0^\circ$ (only resist extension), $\tau = 45^\circ$ (resist extension and compression equally) and $\tau = 90^\circ$ (only resist compression).

In Figure 5 we see how the stiffer the fibres (the larger S), the earlier the onset of surface-wrinkles. This same effect was noticed for simple shear [16, 25]. The dashed lines show when the fibres are along the direction of greatest stretch $A = 45^\circ$ and greatest compression $A = 90^\circ + 45^\circ$. We see that the most distinctive difference is that fibres that only resist extension wrinkle earlier when $A = 45^\circ$, while in comparison the fibres that only resist compression wrinkle earlier when $A = 90^\circ + 45^\circ$.

Figure 4*b*, showing A against θ^*, is harder to interpret. What relationship could one expect between the angle of the fibres before deformation A and the angle of the wrinkle-front θ^* after

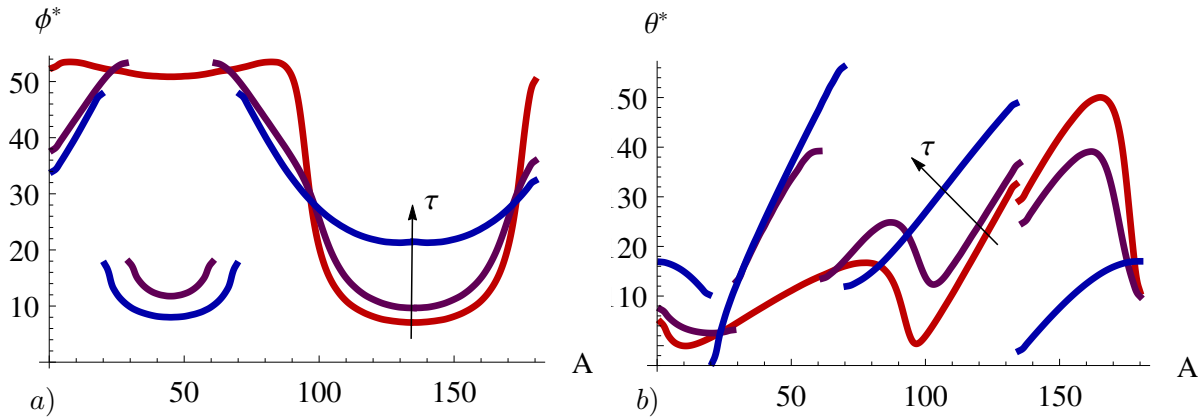

Figure 4. The graphs show the critical deformation ϕ^* and wrinkle-front angle θ^* for a surface-wrinkle to appear with fibre angle A degrees from the X_1 axes. The material parameters used were $\mathsf{S} = 16$, $C_1 = 1$, $C_2 = 0$, $C_3 = 200$ and $\tau = 0°$, $45°$ and $90°$ correspond to the red, purple and blue curves, respectively.

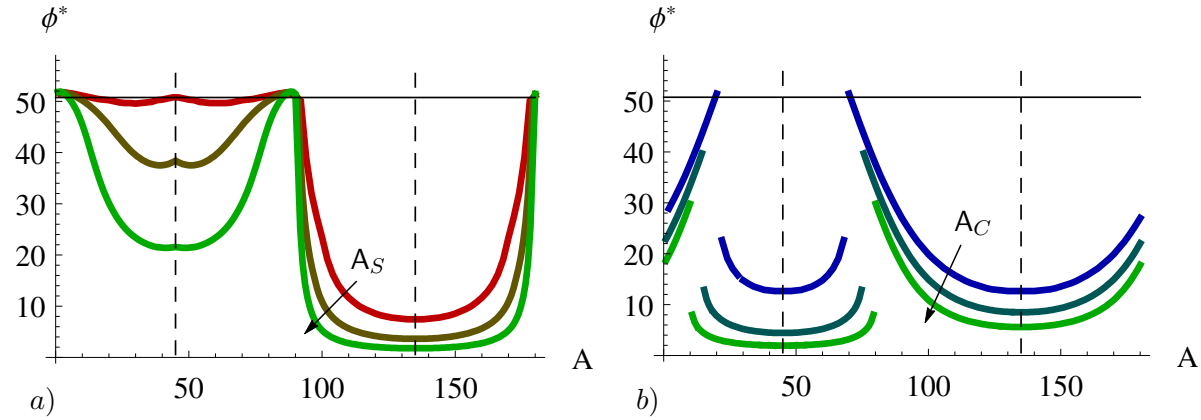

Figure 5. *a*) and *b*) are graphs of the onset of surface-wrinkles for fibres that only resist extension ($\tau = 0$) and compression ($\tau = \pi/2$), respectively. For both plots, as the curves shade towards green, S takes the values 16, 32 and 64. The dashed lines show when the fibres are most stretched ($A = 45°$) or most compressed ($A = 90° + 45°$). The solid black line $\phi^* = 50.75°$ shows when a wrinkle would appear if there were no fibres.

deformation? We can make better sense of these results by using the current angle of the fibres α_S, and the compression counterpart α_C. To find these angles we need $\mathbf{F}_{ij} = \partial x_i/\partial X_j$, with x_i's for the shear-box given by Equations (30). Then α_S and α_C are respectively the angles that $\mathbf{m}^S = \mathbf{FM}$ and $\mathbf{m}^C = \mathbf{F}^{-T}\mathbf{M}$ make with x_1 axes,

$$\alpha_S = \tan^{-1}\left(\frac{\tan A \cos\phi}{\tan A \sin\phi + 1}\right) \quad \text{and} \quad \alpha_C = \tan^{-1}\left(\frac{\tan A - \sin\phi}{\cos\phi}\right). \tag{32}$$

Looking at $\mathcal{A}^A_{ijkl}$ in equation (17) we can clearly see the importance of $\mathbf{m}^S$ and $\mathbf{m}^C$. Their angles can be understood qualitatively through the maps $A \to \alpha_S(A,\phi)$ and $A \to \alpha_C(A,\phi)$, where we can imagine that ϕ is fixed. When the fibres are along the direction of greatest stretch in the reference, $A = 45°$, both these maps bring $45°$ to the angle of greatest stretch in the current configuration. The same applies to the direction of greatest compression, that is both α_S and α_C map $45° + 90°$ to the angle of least stretch in the current configuration. In general $A \to \alpha_S(A,\phi)$ takes points close to $A = 45°$ and brings them even closer to $\alpha_S(45°,\phi)$, while it takes points close to $A = 45° + 90°$ and repels them from $\alpha_S(45°,\phi)$. The map $A \to \alpha_C(A,\phi)$ has the opposite effect.

Using these maps and the same parameter range in Figure 5 we produce two new plots: Figure 6*a* shows α_S against θ^* for fibres that resist extension and Figure 6*b* shows α_C against θ^* for fibres that resist compression. These graphs have multiple discontinuities and are even at times multivalued. From the theory there is no guarantee of a unique wrinkle-front angle θ^* and seemingly the stiffer the fibres, the more competing minima for θ^* appear. Figure 6 shows how the wrinkle-front angle θ^* changes as the fibres become stiffer (S increases). These graphs show a clear trend. In Figure 6*a* the angle between α_S and θ^* alternates between being close to the three quanta $\theta^* - \alpha_S = 90°$, $33.3°$ and $-33.3°$. Similarly, in Figure 6*b* the angle between α_C and θ^* alternates between the three quanta $\theta^* - \alpha_S = 0°$, $55°$ and $-55°$. In both cases the stiffer the fibres, the more closely $\theta^* - \alpha_S$ and $\theta^* - \alpha_C$ stay on their respective quanta. These same quanta, for both cases, seem not to change as C_2/C_1 is increased from 0% to 100%.

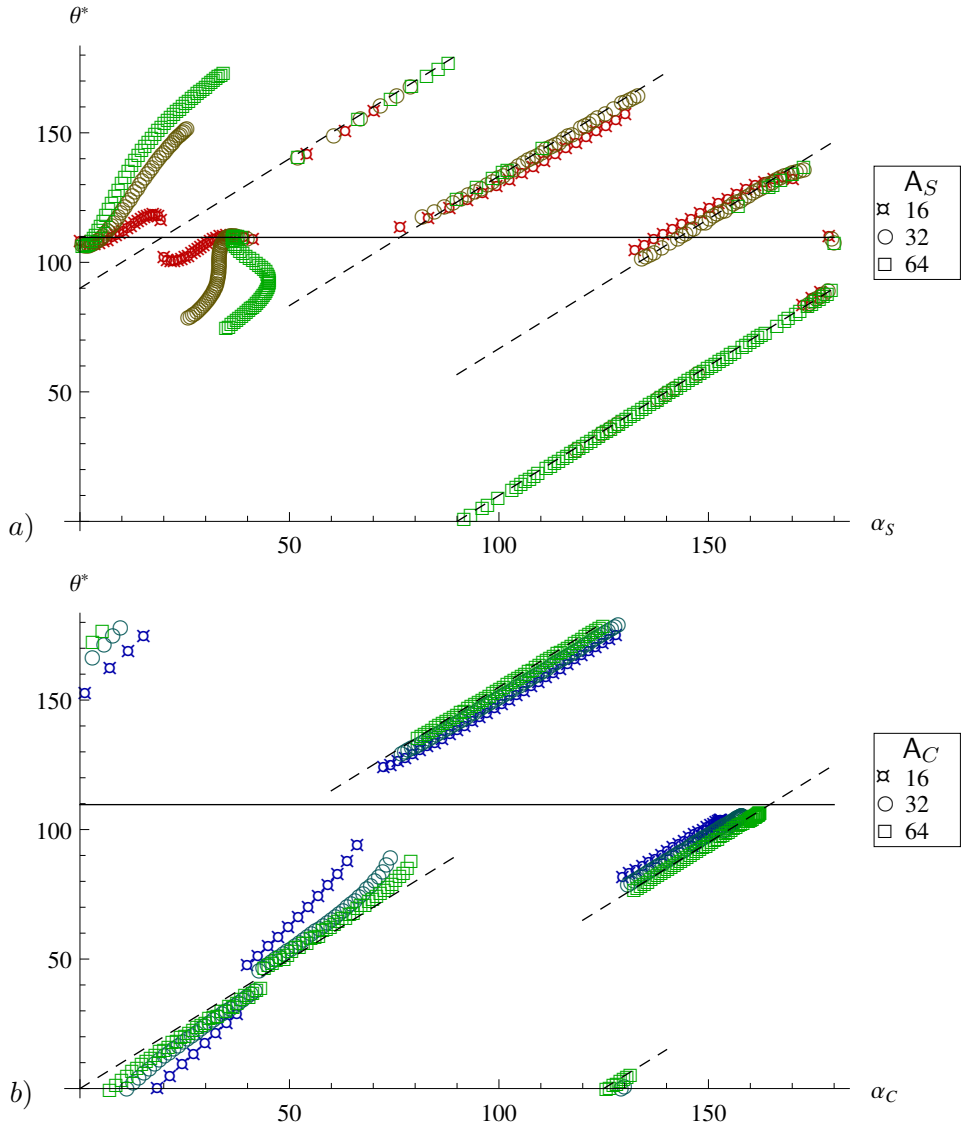

Figure 6. *a*) is a graph of the current fibre angle α_S against the wrinkle-front angle θ^* for a material with fibres that only resist extension. The dashed lines are either $\theta^* - \alpha_S = 90°$, $33.3°$ or $-33.3°$. *b*) is a graph of the current compressive fibre angle α_C against the wrinkle-front angle θ^* for a material with fibres that only resist compression. The dashed lines are either $\theta^* - \alpha_S = 0°$, $55°$ or $-55°$. In both cases the solid black line is given by $\theta^* = 109.6°$ and is the wrinkle-front angle if there were no fibres.

The question that remains is how fibres with both $\mathsf{A}_S \neq 0$ and $\mathsf{A}_C \neq 0$ will behave. Figure 7 answers that question, where $\mathsf{A}_S = \mathsf{A}_C = 64\cos 45°$ and we have varied the value of C_2 so as to illustrate that C_2 hardly affects the quanta. This time both the graphs (α_S, θ^*) and (α_C, θ^*) are similar, and both gravitate around the quanta $\theta^* - \alpha_C = 0°$, $55°/2 + 33.3°/2$, $90°$ and $-55°/2 - 33.3°/2$. For this reason Figure 7 only shows (α_C, θ^*). Note that as C_2 decreases the fibres get comparatively stiffer than the isotropic matrix and again the curves get closer to the dashed lines. The values $55°/2 + 33.3°/2$ and $-55°/2 - 33.3°/2$ are half way between two of the quanta for $\mathsf{A}_S = 0$ and two of the quanta for $\mathsf{A}_C = 0$, which indicates that a simple rule relating A_S and A_C to the resulting quanta probably exists.

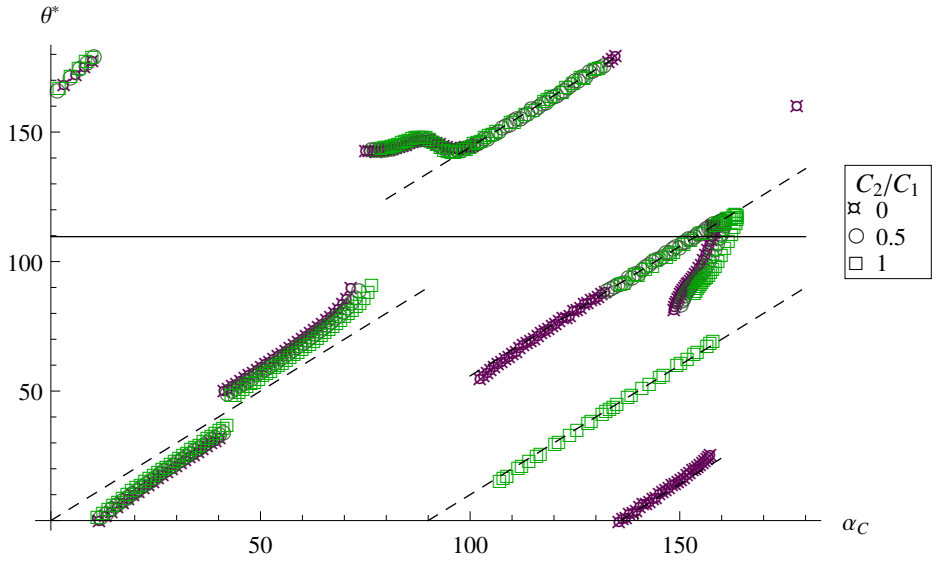

Figure 7. Shows a graph of (α_C, θ^*) for fibres with $\mathsf{A}_S = \mathsf{A}_C = 64\cos 45°$. The dashed lines are either $\theta^* - \alpha_C = 0°$, $90°$, $33.3°/2 + 55°/2$ or $-33.3°/2 - 55°/2$. The solid black line is given by $\theta^* = 109.6°$ and is the wrinkle-front angle if there were no fibres.

3.4. Asymptotics

We have found that varying the fibres' resistance to compression and extension greatly changes the surface wrinkle-front angle. So it is possible to characterize the fibres through the formation of surface wrinkles, but the calculations to do so are quite demanding. If approximations could be developed to extract the key features in the wrinkling pattern, it might be enough to characterize the fibres without computing the complete wrinkling graphs.

Based on the numerical experiments of Section 3.3, an attractive choice is to approximate $\alpha_S - \theta$, or $\alpha_C - \theta$, defined by Equations (32), as being constant. A further simplification is to only investigate fibres that are approximately along the most and least stretched directions. For it is in these directions that a change in A_S and A_C most affects the critical deformation ϕ^*. Another reason to make this simplification is that for simple shear, α_S becomes asymptotic to the direction of greatest stretch [25] when $\alpha_S - \theta \approx 90°$.

Here we will only indicate how to formulate these approximations for a general homogeneous deformation. To simplify the calculations, we choose a coordinate system such that the deformation gradient $\mathbf{F}$ is diagonalized, with $F_{ii} = \lambda_i$ for $i = 1, 2, 3$ and the λ_i's are the principal stretches. Let $\lambda_3 > \lambda_1$ and let λ_2 correspond to a stretch which is orthogonal to the plane of the fibres, so that $\mathbf{M} = (\cos A, 0, \sin A)$. This way the current fibre angles α_S and α_C, measured

from the x_1 axis, are

$$\alpha_S = \arctan\left(\frac{\lambda_3 \sin A}{\lambda_1 \cos A}\right) \quad \text{and} \quad \alpha_C = \arctan\left(\frac{\lambda_1 \sin A}{\lambda_3 \cos A}\right). \tag{33}$$

As an example, we will approximate α_C as being the angle of the direction of greatest stretch and approximate $\theta - \alpha_C = 0$, this would respectively translate to

$$\alpha_C = \pi/2 + \delta\alpha\,\pi \quad \text{and} \quad \alpha_C = \theta + \epsilon\pi, \tag{34}$$

for $\delta\alpha$ and ϵ small. Both these approximations hold true for a portion of every numerical experiment discussed in Section 3.3. From the first of these approximations we deduce that,

$$\cos A = \pm\delta\alpha\,\pi\frac{\lambda_1}{\lambda_3} + \mathcal{O}(\delta\alpha^3) \quad \text{and} \quad \sin A = 1 - \frac{\pi^2\delta\alpha^2}{2}\frac{\lambda_1^2}{\lambda_3^2} + \mathcal{O}(\delta\alpha^3). \tag{35}$$

From both approximations (34) we deduce that $\theta = \pi/2 + (\delta\alpha - \epsilon)\pi$, where we rename $\delta\alpha - \epsilon = \delta\theta$, resulting in

$$\cos\theta = -\delta\theta\pi + \mathcal{O}(\delta\theta^3) \quad \text{and} \quad \sin\theta = 1 - \frac{\delta\theta^2\pi^2}{2} + \mathcal{O}(\delta\theta^3). \tag{36}$$

Suppose that λ_1, λ_2 and λ_3 are parametrized by some magnitude of deformation φ. These approximations can then be used in the incremental moduli $\mathcal{A}_{ijkl}$, from which we obtain the matrices $\mathbf{T} = \mathbf{T}(\delta\alpha, \delta\theta, \varphi)$, $\mathbf{R} = \mathbf{R}(\delta\alpha, \delta\theta, \varphi)$ and $\mathbf{Q} = \mathbf{Q}(\delta\alpha, \delta\theta, \varphi)$ for the Riccati equation (27). Truncating the resulting Riccati equation for some order in $\delta\alpha$ and $\delta\theta$ may lead to analytic results, or at least greatly simplify the application of the Riccati method 3.2, as both $\delta\alpha$ and $\delta\theta$ need only have a small range.

4. Conclusion

There is a clear need for more complete models of fibre reinforced materials. Here we have pointed a way to include both anisotropic invariants in a simple physical way: through one invariant that measures fibre stretch I_4^S and another that measures fibre compression I_4^C. Giving a clear meaning to the anisotropic invariants makes it is easier to design specific models, and perhaps to fit parameters from experiments, as varying A_S and A_C dramatically changes the material's response. We also explained a method for using the Riccati equation to calculate surface wrinkles.

A striking phenomena was revealed when studying the onset of surface-wrinkles: the difference between the current fibre orientation and the wrinkle orientation $\alpha_S - \theta^*$, and $\alpha_C - \theta^*$, tends to only occupy 3 or 4 possible discrete values, see Figure 7. This simple behaviour must have a simple underlying explanation. One possible avenue would be to develop asymptotic solutions, as suggested in Section 3.4. Explaining this quanta phenomena could lead to a simple method for approximately calculating surface wrinkles for anisotropic materials, and therefore lead to an efficient way to characterize fibre reinforced soft solids by how they form surface-wrinkles.

Acknowledgements

The support of the Hardiman Foundation (NUI Galway) and of the Irish Research Council is gratefully acknowledged. I thank Konstantine Soldatos and Raymond Ogden for their support, and for organizing Euromech Colloquium 551: "Fibre-reinforced Materials: Theory and Applications". I thank Michel Destrade for insightful discussions and support.

References

1. J. C. Criscione, I. Lorenzen-Schmidt, J. D. Humphrey, and W. C. Hunter, "Mechanical contribution of endocardium during finite extension and torsion experiments on papillary muscles," *Annals of biomedical engineering*, vol. 27, no. 2, pp. 123–130, 1999.
2. P. S. Donzelli, R. L. Spilker, G. A. Ateshian, and V. C. Mow, "Contact analysis of biphasic transversely isotropic cartilage layers and correlations with tissue failure," *Journal of Biomechanics*, vol. 32, pp. 1037–1047, Oct. 1999.
3. A. Spencer, *Constitutive theory for strongly anisotropic solids*. Springer-Verlag, 1984.
4. G. a. Holzapfel and R. W. Ogden, "Constitutive modelling of arteries," *Proceedings of the Royal Society A: Mathematical, Physical and Engineering Sciences*, vol. 466, pp. 1551–1597, Mar. 2010.
5. J. Lu and L. Zhang, "Physically motivated invariant formulation for transversely isotropic hyperelasticity," *International Journal of Solids and Structures*, vol. 42, pp. 6015–6031, Nov. 2005.
6. P. Ciarletta, I. Izzo, S. Micera, and F. Tendick, "Stiffening by fiber reinforcement in soft materials: A hyperelastic theory at large strains and its application," *J. Biomech. Behavior Biomed. Mat.*, vol. 4, pp. 1359–1368, 2011.
7. J. Murphy, "Transversely isotropic biological, soft tissue must be modelled using both anisotropic invariants," *European Journal of Mechanics - A/Solids*, vol. 42, pp. 90–96, Nov. 2013.
8. M. Destrade, B. M. Donald, J. G. Murphy, and G. Saccomandi, "At least three invariants are necessary to model the mechanical response of incompressible, transversely isotropic materials," *Computational Mechanics*, vol. 52, pp. 959–969, Apr. 2013.
9. E. Pucci and G. Saccomandi, "On the use of universal relations in the modeling of transversely isotropic materials," *International Journal of Solids and Structures*, vol. 51, pp. 377–380, Jan. 2014.
10. M. Van Loocke, C. Lyons, and C. Simms, "A validated model of passive muscle in compression," *Journal of Biomechanics*, vol. 39, p. 29993009, 2006.
11. C. P. Brangwynne, F. C. MacKintosh, S. Kumar, N. A. Geisse, J. Talbot, L. Mahadevan, K. K. Parker, D. E. Ingber, and D. A. Weitz, "Microtubules can bear enhanced compressive loads in living cells because of lateral reinforcement," *Journal of Cell Biology*, 2006.
12. J. Merodio and R. Ogden, "Instabilities and loss of ellipticity in fiber-reinforced compressible non-linearly elastic solids under plane deformation," *International Journal of Solids and Structures*, vol. 40, pp. 4707–4727, Sept. 2003.
13. G. Holzapfel, T. Gasser, and R. Ogden, "A new constitutive framework for arterial wall mechanics and a comparative study of material models," *Journal of elasticity and the physical science of solids*, vol. 61, no. 1-3, pp. 1–48, 2000.
14. G. A. Holzapfel and R. W. Ogden, "On planar biaxial tests for anisotropic nonlinearly elastic solids. a continuum mechanical framework," *Mathematics and Mechanics of Solids*, vol. 14, 2009.
15. S. Mora, M. Abkarian, H. Tabuteau, and Y. Pomeau, "Surface instability of soft solids under strain," *Soft Matter*, vol. 7, no. 22, p. 10612, 2011.
16. M. Destrade, M. D. Gilchrist, D. a. Prikazchikov, and G. Saccomandi, "Surface instability of sheared soft tissues.," *Journal of biomechanical engineering*, vol. 130, p. 061007, Dec. 2008.
17. Y. B. Fu and A. Mielke, "A new identity for the surface-impedance matrix and its application to the determination of surface-wave speeds," *Proceedings of the Royal Society A: Mathematical, Physical and Engineering Sciences*, vol. 458, pp. 2523–2543, Oct. 2002.
18. Y. Fu, "An integral representation of the surface-impedance tensor for incompressible elastic materials," *Journal of Elasticity*, vol. 81, no. 1, pp. 75–90, 2005.
19. B. Li, Y.-P. Cao, X.-Q. Feng, and H. Gao, "Mechanics of morphological instabilities and surface wrinkling in soft materials: a review," *Soft Matter*, vol. 8, no. 21, pp. 5728–5745, 2012.
20. J. Genzer and J. Groenewold, "Soft matter with hard skin: From skin wrinkles to templating and material characterization," *Soft Matter*, vol. 2, no. 4, pp. 310–323, 2006.
21. A. L. Gower, M. Destrade, and R. Ogden, "Counter-intuitive results in acousto-elasticity," *Wave Motion*, vol. 50, 2013.
22. M. B. Amar and A. Goriely, "Growth and instability in elastic tissues," *Journal of the Mechanics and Physics of Solids*, vol. 53, pp. 2284–2319, 2005.
23. V. Balbi and P. Ciarletta, "Morpho-elasticity of intestinal villi," *J. R. Soc. Interface*, 2013.
24. C. M. Stafford, C. Harrison, K. L. Beers, A. Karim, E. J. Amis, M. R. VanLandingham, H.-C. Kim, W. Volksen, R. D. Miller, and E. E. Simonyi, "A buckling-based metrology for measuring the elastic moduli of polymeric thin films.," *Nature materials*, vol. 3, pp. 545–50, Aug. 2004.
25. P. Ciarletta, M. Destrade, and A. L. Gower, "Shear instability in skin tissue," *The Quarterly Journal of Mechanics and Applied Mathematics*, vol. 2, pp. 273–288, 2013.
26. R. W. Ogden, *Nonlinear Elastic Deformations*. Dover New York, 1997.
27. J. E. Marsden and T. J. R. Hughes, *Mathematical Foundations of Elastictiy*. Dover, 1994.

28. J. R. Walton and J. P. Wilber, "Sufficient conditions for strong ellipticity for a class of anisotropic materials," *International Journal of Non-Linear Mechanics*, vol. 38, pp. 441–455, 2003.
29. T. C. T. Ting, *Anisotropic elasticity: theory and Applications*. Press, Oxford University, 1996.
30. A. Norris and A. Shuvalov, "Wave impedance matrices for cylindrically anisotropic radially inhomogeneous elastic solids," *Q. J. Mech. Appl. Math.*, vol. 63, pp. 401–435, 2010.
31. A. J. Laub, "A Schur method for solving algebraic Riccati equations," *Automatic Control, IEEE Transactions on*, vol. 24, pp. 913–921, Dec. 1979.
32. P. Benner and R. Byers, "An exact line search method for solving generalized continuous-time algebraic Riccati equations," *Automatic Control, IEEE Transactions on*, vol. 43, pp. 101–107, Jan. 1998.
33. A. Norris, A. Shuvalov, and a.a. Kutsenko, "The matrix sign function for solving surface wave problems in homogeneous and laterally periodic elastic half-spaces," *Wave Motion*, vol. 50, pp. 1239–1250, Dec. 2013.
34. A. Mielke and Y. Fu, "A proof of uniqueness of surface waves that is independent of the stroh formalism," *Mathematics and Mechanics of Solids*, vol. 9, pp. 5–15, 2003.
35. C. Stolz, *Milieux Continus en Transformations Finies*. Editions de l'Ecole Polytechnique, 2010.
36. S. Roccabianca, M. Gei, and D. Bigoni, "Plane strain bifurcations of elastic layered structures subject to finite bending: theory versus experiments," *IMA journal of applied mathematics*, vol. 75, no. 4, pp. 525–548, 2010.